JOURNAL OF GEOPHYSICAL RESEARCH, VOL. 92, NO. D10, PAGES 11,993–11,999, OCTOBER 20, 1987

A Saturated Inertia Gravity Wave in the Mesosphere Observed by the Middle and Upper Atmosphere Radar

MAMORU YAMAMOTO, TOSHITAKA TSUDA, SUSUMU KATO, TORU SATO, AND SHOICHIRO FUKAO

Radio Atmospheric Science Center, Kyoto University, Uji, Kyoto, Japan

We have found the dominance of a monochromatic inertia gravity wave with a vertical wavelength of approximately 5.6 km from middle and upper atmosphere radar observations of the mesosphere on February 8, 1985. By assuming linear dispersion and polarization equations for gravity waves, we have estimated the intrinsic period and propagation direction of the wave as 8 hours and northward, respectively. The minimum Richardson number for the atmosphere as modified by the inertia gravity wave was slightly negative near 72 km, which implies that the wave was saturated and generated turbulence through shear and convective instabilities. We observed an echo power enhancement near the altitude of the minimum Richardson number. At 68–78 km altitude we found intermittent fluctuations in radial wind velocities with a period of 9 min. Their phases rapidly reversed near 73 km, where their amplitudes reached a minimum and the Richardson number was less than 1. These fluctuations seem to be attributable to the shear or convective instabilities generated by the saturating gravity wave.

INTRODUCTION

Observations show that gravity waves in the middle atmosphere dissipate and lose their energy through an instability process [*Manson et al.*, 1979; *Vincent and Stubbs*, 1977; *Vincent*, 1984]. *Hodges* [1967] pointed out that gravity waves could dissipate through convective instabilities when the background potential temperature became superadiabatic. The gravity waves transfer their momentum to accelerate the mean wind [*Lindzen*, 1981]. As discussed by *Fritts and Rastogi* [1985], one of the dynamical instabilities in the atmosphere is the Kelvin-Helmholtz instability, which sets in when the Richardson number of the wind profile is less than $\frac{1}{4}$ [*Drazin*, 1958]. It is very important to observe the relation between gravity waves and instabilities in order to understand the dynamics of the middle atmosphere.

By using Doppler radars, *Van Zandt et al.* [1979] and *Klostermeyer and Rüster* [1980, 1981] observed fluctuations of radial wind velocities with rapid phase jumps at certain altitudes. Through comparison with model calculations these fluctuations were attributed to Kelvin-Helmholtz instabilities induced by a shear at the bottom of the jet stream. In mesosphere observations, *Klostermeyer and Rüster* [1984] reported echo power bursts and simultaneous oscillations of radial velocity at the maximum shear of the wave structure of the background wind. Although these oscillations were attributed to a Kelvin-Helmholtz instability, *Klostermeyer and Rüster* [1984] did not show the amplitude and phase profiles of the fluctuation. With the middle and upper atmosphere (MU) radar (35°N, 135°E), *Yamamoto et al.* [1987] found three examples of gravity waves in the mesosphere which were related to scattering layers. They showed that the downward motion of scattering layers was similar to the vertical phase velocity of the gravity waves and the maximum echo power appeared at the altitude of the minimum Richardson number for the atmosphere, which is modified by the gravity waves. We call the waves inertia gravity waves because their intrinsic period was comparable to the inertial period. One of the examples showed an inertia gravity wave with a negative Richardson number and large fluctuations in radial wind velocities. In this paper we will discuss the relations among the gravity wave, the fluctuations, and the echo power in more detail.

Paper number 7D0579.
0148-0227/87/007D-0579$05.00

RESULTS OF THE OBSERVATION

Inertia Gravity Wave

The MU radar has been in operation since 1983. This system is described in detail by *Kato et al.* [1984] and *Fukao et al.* [1985*a*, *b*]. Observations of the mesosphere were carried out on February 8, 1985, using the parameters shown in Table 1. We used four beams, pointing northward, eastward, southward, and westward, each with a zenith angle of 10°. We steered the beam during every interpulse period, and 30 successive echoes were coherently integrated. This corresponds to a sampling interval of 87.6 ms, and the Nyquist limit of the radial wind velocity was 18.4 m s^{-1}. Ten successive power spectra of the received signal were incoherently integrated and stored on magnetic tapes every 2 min. By taking into account the vertical wind velocity, the eastward and northward components of wind velocities were calculated from the average of the pair of radial wind velocities measured in east-west and north-south directions, respectively.

Figure 1 shows horizontal wind profiles, each of which is a 2-hour average determined every hour. The dashed lines are the vertical linear trends. The trends of the northward wind velocities lie between −30 and 30 m s^{-1} and show a northward shear of approximately 4.5 m s^{-1} km^{-1}. The vertical linear trends of the eastward wind velocities lie between 10 and 50 m s^{-1} with an eastward shear of approximately 3.5 m s^{-1} km^{-1} in the first three profiles. The eastward wind profiles at 1400 and 1500 LT, however, exceed 50 m s^{-1} at altitudes above 75 km. These data seem to be contaminated because of the weak echo power, and we exclude eastward wind profiles after 1400 LT from the following discussions. Until 1400 LT, all northward and eastward wind profiles clearly show a monochromatic wavelike structure superposed on each vertical linear trend. We note that the amplitude of the wavelike structure is large and comparable to the range of the vertical linear trend of the wind profile. The vertical phase velocity of the wave is approximately 0.4 km h^{-1}, which is estimated by

TABLE 1. Observation Parameters of the MU Radar

Parameter	Value
Observation period	February 8, 1985
Observation range, km	60–98.1
Number of beams	4
Zenith angle θ, deg	
Northward beam direction	10
Eastward beam direction	10
Southward beam direction	10
Westward beam direction	10
Range resolution, m	300
Time resolution, s	120
Interpulse period, μs	730
Pulse compression	16 bit complementary
Coherent integration	30 times
Incoherent integration	10 times

using the northward wind profiles. From the profile at 1300 LT the vertical wavelength is approximately 5.6 km, and the apparent period is approximately 13 hours. The vertical wavelength seems to be too short for that of the fundamental modes of semidiurnal tides usually detected in the mesosphere [*Kato*, 1980]. By using the data obtained by the Kyoto meteor radar, we found that in February 1985 the wavelength of the semidiurnal tide was 75 km in the altitude range of 80–110 km. The amplitudes of the semidiurnal and diurnal tides were both less than 10 m s^{-1} in the altitude range of 80–90 km, which agree with seasonal variation of semidiurnal tides detected by the Kyoto meteor radar (R. A. Vincent et al., A comparative study of mesospheric solar tides observed at Adelaide and Kyoto, submitted to *Journal of Geophysical Research*, 1987). We would infer that the wave shown in Figure 1 is not largely affected by semidiurnal tides but is a manifestation of inertia gravity waves.

In order to investigate the polarization of the wave a height profile of the wind velocity vector is calculated by averaging the eastward and northward components obtained during

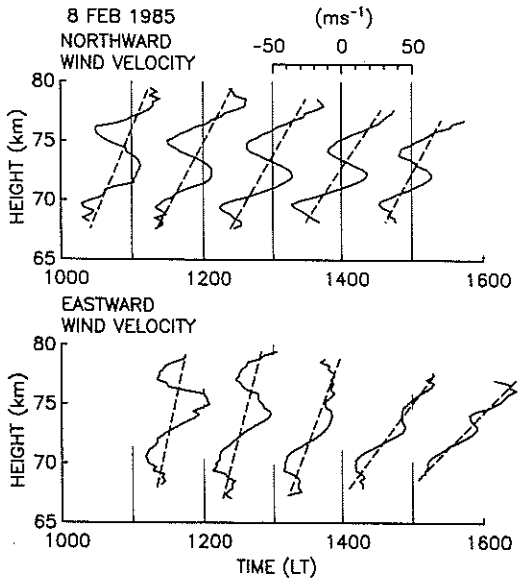

Fig. 1. Northward (top) and eastward (bottom) wind profiles observed on February 8, 1985. Each profile is averaged over 2 hours with 1 hour overlap. Dashed lines show linear trends of each wind profile.

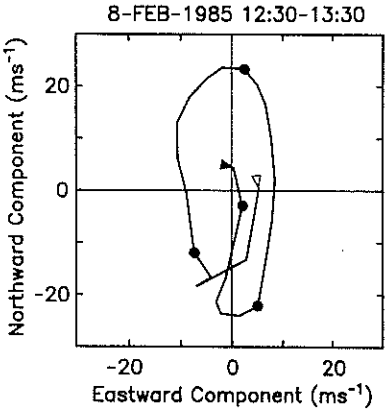

Fig. 2. A polar plot of the wind velocity averaged over 1230–1330 LT on February 8, 1985. Vertical linear trend of the wind profile is subtracted. The open and solid triangles on the solid line indicate the lowest (68.8 km) and highest altitudes (76.5 km). Circular symbols are ploted at 70, 72, 74, and 76 km.

1230–1330 LT. Figure 2 shows a hodograph of the wind vector after subtracting the vertical linear trend of the profile. The tip of the wind vector moves clockwise with increasing height throughout the whole altitude range. Especially, it shows a clear elliptical motion with a long axis along the north-south direction below 74 km. This suggests that the wave is an inertia gravity wave which propagates its energy upward [*Gossard and Hooke*, 1975]. From the ratio between the long and short axes of the ellipse the intrinsic period of the wave is estimated to be approximately 8 hours. The gravity wave appears to propagate in the vertical plane that makes an angle of 7° eastward from the north. As mentioned above, the apparent period of the gravity wave is approximately 13 hours, which is longer than the intrinsic period of 8 hours. The difference between those periods seems to be due to the Doppler effect, which shows that the gravity wave must be propagating against the northward component of the background wind. Although the direction of the background wind changes within the altitude range, the northward components of the vertical linear trends are negative below 74 km in the region where the hodograph shows clear elliptical motion. Assuming that the vertical linear trend of the wind profile represents the background wind velocity, we infer that the gravity wave propagates northward. According to the dispersion equation for gravity waves the horizontal wavelength is approximately 600 km, and the background wind velocity should be -8 m s^{-1} to produce the Doppler effect of the wave. This southward wind is realized around 72 km at 1300 LT.

Short-Period Fluctuations

We have calculated the power spectral density of radial velocities in order to investigate the fine structure of the wind field. Figure 3 shows a contour plot of the power spectra in the southward beam. Although the longer-period components generally have higher densities than the shorter components, there is one distinct component with an 8- to 10-min period evident throughout the altitude range. This component is intense at 68–72 km and 74–78 km altitude and weak around 73 km. Figure 4 shows radial wind velocities in the same beam direction. Components with periods of 6–16 min are picked out by means of a numerical band-pass filter. In the altitude regions lower than 72 km and higher than 74 km, fluctuations

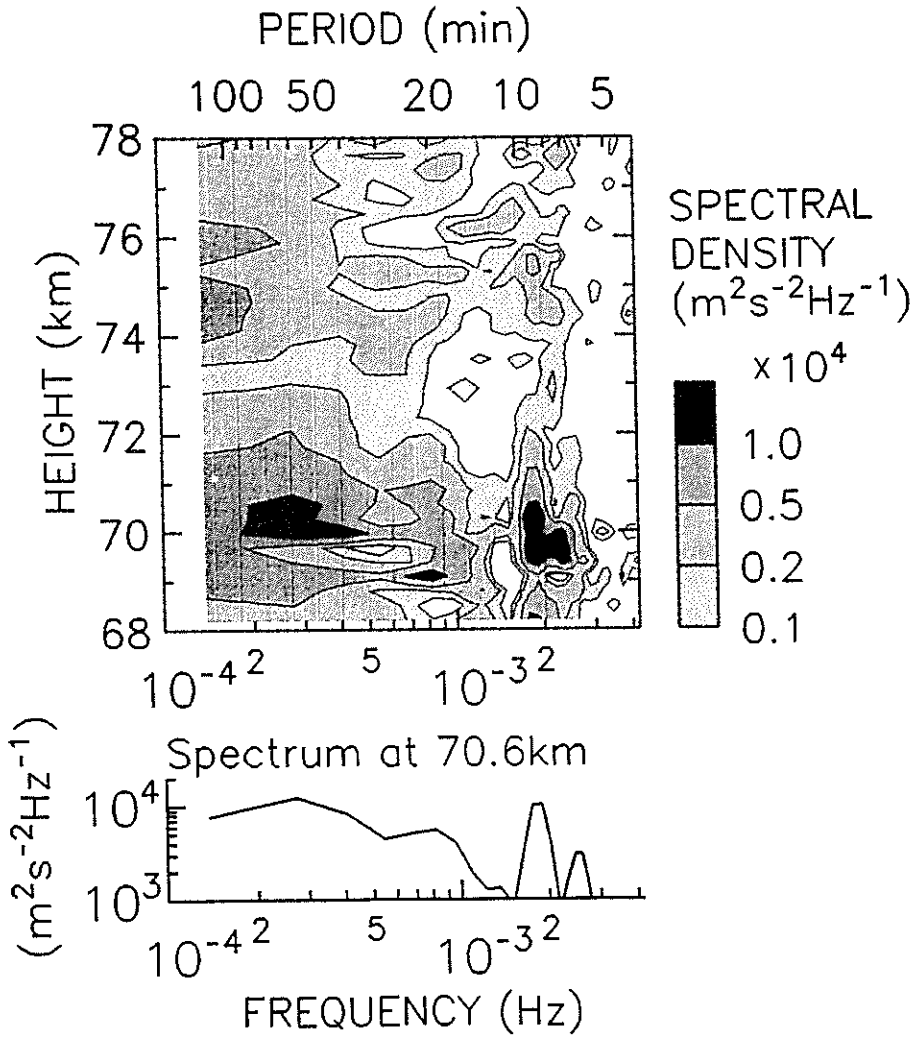

Fig. 3. The top panel shows the height distribution of power spectral densities of radial wind fluctuations observed during 1000–1600 LT in the southward beam on February 8, 1985. The bottom panel shows the power spectrum obtained at 70.6 km.

are intense, and the maximum amplitude of the fluctuation is approximately 5 m s^{-1}. The phases of the fluctuations are almost constant with height above and below 73 km, and the amplitude seems to be smallest at 73 km. We also note that there is a sudden phase reversal at the altitude of the smallest amplitude. In Figure 5 we compare the radial wind velocities at altitudes the same distance above and below 73 km. The signs of one of the radial wind velocities are reversed, and the positive values shown for the data obtained above and below 73 km correspond to approaching and receding velocities, respectively. The radial wind velocities at the two altitude

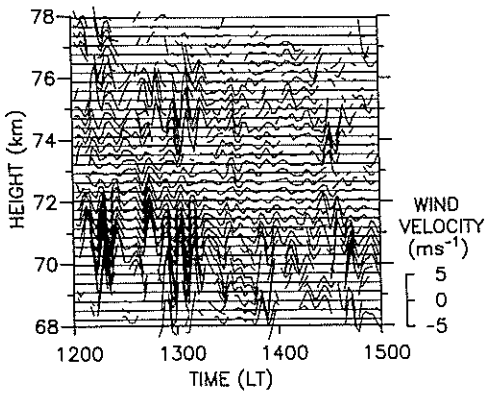

Fig. 4. Radial wind fluctuations with periods ranging from 6 to 16 min observed in the southward beam on February 8, 1985.

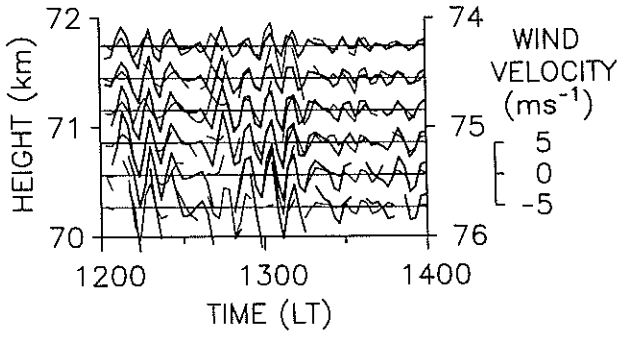

Fig. 5. Radial wind variations at altitudes the same distances above and below the phase reversal height (73 km), with the sign of one reversed. Thick lines show the variations below 73 km with receding positive, and thin lines show those above 73 km with approaching positive. The left and right vertical axes show the altitudes below and above 73 km, respectively.

ranges seem to be not only phase reversed, but also show very similar time variations with each other. This is especially clear when the amplitude becomes large.

Rastogi and Bowhill [1976] and *Fukao et al.* [1979] observed radial wind fluctuations in the mesosphere with periods of 10–15 min and amplitudes of less than 2 m s^{-1}. They explained these oscillations in terms of evanescent surface waves with periods near the Brunt-Väisälä frequency. The fluctuations shown in Figure 4, on the other hand, have a clear phase reversal near 73 km, which was not observed in the oscillations mentioned above. Furthermore, the symmetrical nature of the fluctuations above and below 73 km strongly suggests that they belong to one system of instabilities which covers the altitude range of 68–78 km.

Figure 6 illustrates the rms speeds of the radial wind fluctuations averaged in two altitude regions, i.e., 70–72 and 74–76 km. The rms speed in the lower region is larger than that in the upper region, and the maximum values seem to be approximately 3 and 2 m s^{-1} in the lower and upper regions, respectively. They show a similar variation and simultaneously become large for approximately 20 min. We recognize four events of large fluctuations, the first three of which occur periodically during 1205–1320 LT.

In order to investigate the amplitude and the phase of these fluctuations we assumed a sinusoidal oscillation with a period of 9 min and fit it to the radial wind velocities for each event by using the least squares method. Figure 7 shows the amplitudes and phases of the fluctuations for the four events. The origin of phase is arbitrary. Considering that the estimation error of the phase is approximately $\pm 20°$, it is clear that in each event the phase jumps almost 180° within one or two range gates (i.e., 300–600 m) near the altitude where the minimum amplitude occurs. The maximum amplitudes are larger than 5 m s^{-1} and occur at altitudes 3 or 4 km below and above the phase reversal height. The error in the amplitudes is less than ± 1 m s^{-1}. These similarities imply that instabilities of the same kind occur intermittently at slightly different altitudes. In troposphere observations, *VanZandt et al.* [1979] and *Klostermeyer and Rüster* [1980] have reported radial wind oscillations with periods of 4–8 min and phase jumps of approximately 180° and 100°. Although the vertical scale and phase variation of our mesospheric fluctuations are slightly larger than those observed in the troposphere, the behavior seems to be very similar. The Richardson number will be discussed in a later section by taking into account the potential temperature fluctuation due to the inertia gravity wave.

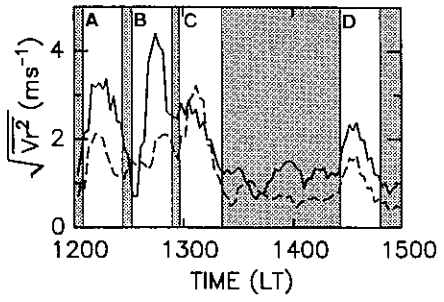

Fig. 6. Variation of rms speed of the radial wind fluctuations V_r' in Figure 4 averaged in the altitude range of 70–72 km (solid line) and 74–76 km (dashed line). A, B, C, and D show events of large fluctuations which occur during 1205–1227, 1232–1254, 1258–1321, and 1424–1446 LT, respectively.

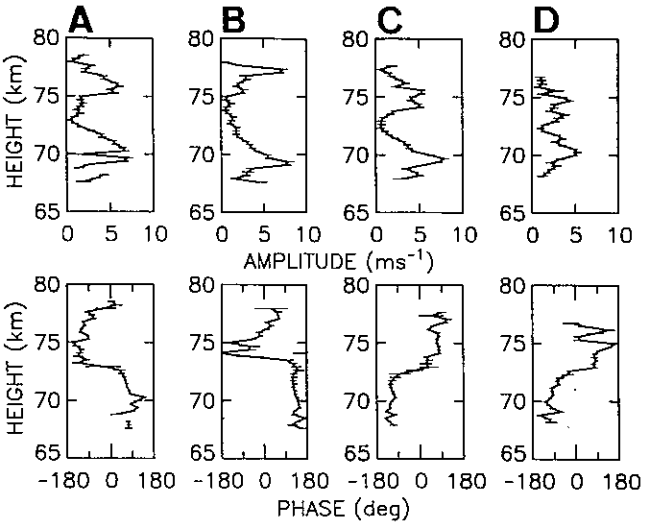

Fig. 7. Amplitude (top) and phase (bottom) profiles of the radial wind fluctuations obtained in each event shown in Figure 6. Radial wind velocities are fitted by assuming a sinusoidal oscillation with a period of 9 min. Error bars on the profile indicate the standard deviation of the estimated amplitudes and phases.

Echo Power and Spectral Width

Figure 8 shows a time-height section of the signal to noise ratio during the observation. Intense scattering layers are shown at 68–80 km; a thin layer at 72 km during 1100–1200 LT seems to be enhanced around 1200 LT and generates a large scattering region during 1200–1600 LT. This turbulent layer consists of many isolated intense patches with thicknesses of 1–2 km and periods of occurrence of several tens of minutes. Most of them seem to move downward. Wavelike structures are shown in the turbulent layers; they are clear during 1400–1530 LT at 70–73 km with a period of approximately 1 hour. Structures with a cat's eye pattern occur within the wavelike structure around 1415 and 1515 LT.

Figure 9 shows profiles of echo power and spectral width (converted to Doppler velocity) averaged over 1230–1330 LT. The echo power is enhanced at both 70–72 and 75–76 km altitudes. Peaks of the echo power near 70 and 75 km agree with those of the amplitude of the radial wind fluctuation shown in Figure 7. It is noted that the echo power is still large at 72–73 km, where the fluctuation amplitude becomes as small as 2 m s^{-1}. The minimum of echo power appears at a slightly higher altitude than the phase reversal in Figure 7. The spectral width is large at the altitudes where the echo power is large and has a minimum of approximately 4 m s^{-1} at altitudes slightly below 74 km. The peak of 8 m s^{-1} around 75 km is larger than that around 71 km. We also find that the spectral width is large in the region with large echo power, which implies that the echo power enhancement is due not to the specular reflection but to turbulence scatter.

As shown in Figure 8, the lower edge of the turbulent layer around 70 km moves up and down. Figure 10 displays the altitude at which the signal to noise ratio is -3 dB, together with the southward radial wind velocity variation at 70.6 km. The fluctuation of the altitude is a measure of the displacement of the lower edge of the turbulent layer. A similar variation of the radial wind velocities between 1200 and 1400 LT is also recognized. A cross correlation between these fluctuations shows that the altitude fluctuation of the turbulence

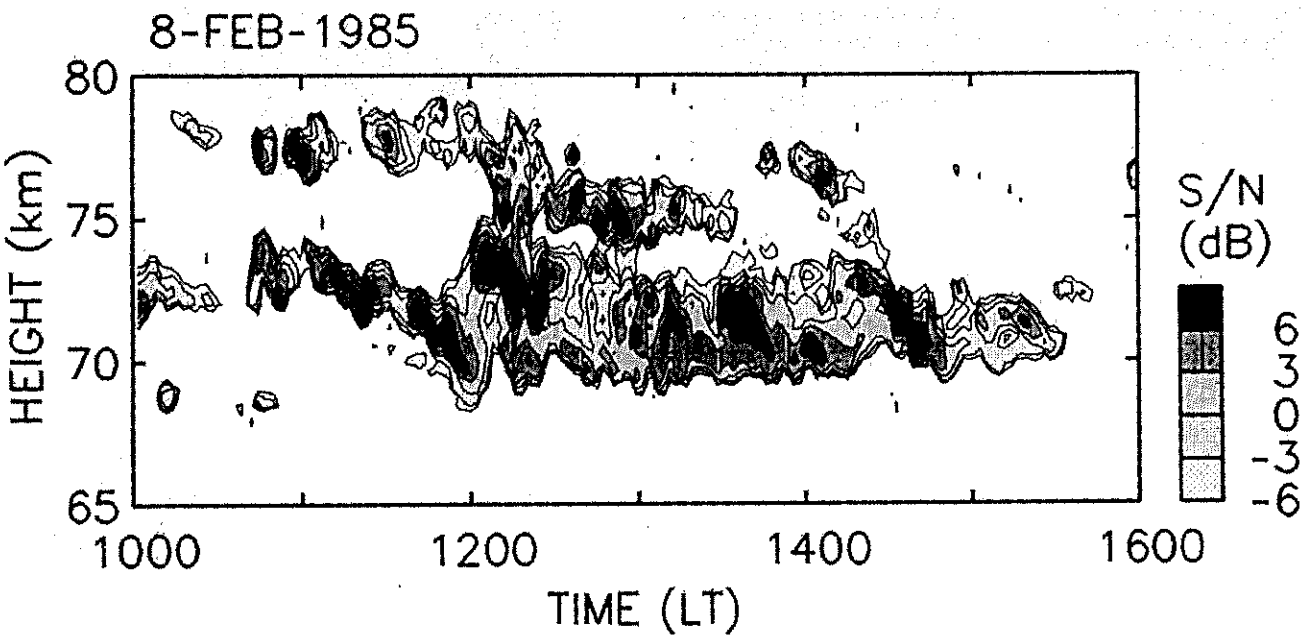

Fig. 8. Time-height sections of the signal to noise ratio observed in the southward beam on February 8, 1985.

layer lags the radial wind fluctuation by approximately 2 min. Because the period of the fluctuation is 9 min, the altitude of the lower edge seems to lag approximately 90° in relation to the radial velocity. With an amplitude of the radial wind fluctuation of about 4 m s^{-1} the vertical displacement is estimated to be 340 m, which is consistent with the amplitude of the altitude fluctuation at around 1300 LT.

Discussion

As is shown in Figure 1, the shear of the wind velocity is mainly due to the inertia gravity waves which are superposed on the background wind. In order to calculate the Richardson number profile we have to take into account the fluctuation of potential temperature induced by the inertia gravity wave as well as the wind shear [*Hodges*, 1967]. *Tsuda et al.* [1985] have studied the importance of the modification of the Richardson number profiles including both wind and temperature fluctuations due to low-frequency gravity waves. According to the linear theory of the gravity waves the polarization equations are

$$v' = -\frac{if}{\omega} u' \tag{1}$$

$$w' = -\frac{k}{m} u' \tag{2}$$

$$\theta' = -\frac{ik}{m\omega} \frac{\partial \bar{\theta}}{\partial z} u' \tag{3}$$

where ω, m, and k are the intrinsic frequency and vertical and horizontal wave numbers of the wave, u' and v' are the fluctu-

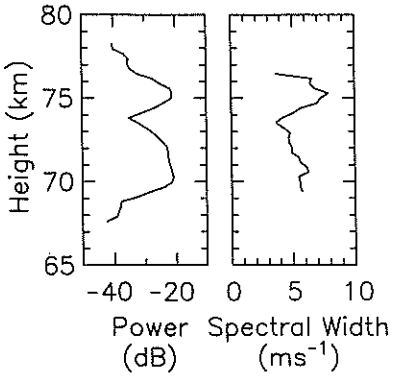

Fig. 9. Profiles of echo power (left panel) and spectral width (right panel) averaged over 1230–1330 LT on February 8, 1985.

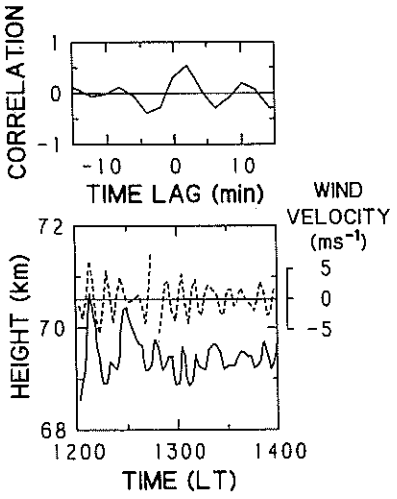

Fig. 10. Altitude variation of the scattering layer and the radial wind velocities in the southward beam (bottom). The solid line shows the variation of altitude of the constant signal to noise ratio contour (−3 dB) around 69.5 km shown in Figure 8. The broken line shows the variation of the radial wind velocity at 70.6 km. The top panel shows the cross-correlation coefficient between the altitude variation and the radial velocity shown in the bottom panel. Positive lag shows that the altitude variation lags in relation to the radial velocities.

ations of the horizontal velocity components along and perpendicular to the propagation direction, w' and θ' are fluctuations of the vertical velocity component and potential temperature, f is the inertial frequency, the overbar denotes the mean, and z is the vertical coordinate [*Fritts and Rastogi*, 1985]. From (3),

$$\frac{\partial \theta'}{\partial z} = -\frac{k}{\omega}\frac{\partial \bar{\theta}}{\partial z}u' \tag{4}$$

The Richardson number Ri is defined as follows:

$$Ri = -\frac{g}{\theta}\frac{\partial \theta}{\partial z}\left[\left(\frac{\partial u}{\partial z}\right)^2 + \left(\frac{\partial v}{\partial z}\right)^2\right]^{-1} \tag{5}$$

where u, v, and θ include both mean and fluctuation and g is the acceleration of gravity. Thus the Richardson number induced by the gravity wave is

$$Ri = -\frac{g}{\bar{\theta}}\frac{\partial \bar{\theta}}{\partial z}\left(1 - \frac{k}{\omega}u'\right)\left[\left(\frac{\partial u}{\partial z}\right)^2 + \left(\frac{\partial v}{\partial z}\right)^2\right]^{-1} \tag{6}$$

By using (6), we have calculated the Richardson number of the wind profile averaged over 1230–1330 LT assuming the wind to be a superposition of the linear trend and the inertia gravity wave which propagates toward the north. Parameters of the calculation are shown in Table 2, where the wave amplitude is assumed to be constant with altitude and the background temperature is taken from the COSPAR International Reference Atmosphere (1972) model. In Figure 11 the calculated wind velocity and shear profiles are shown. Symbols correspond to the observed values. The calculated and observed profiles agree well, especially between 70 and 75 km. The minimum Richardson number is slightly negative around 72 km; this altitude is different from that of the wind shear maxima at 73.2 and 70.5 km because of the potential temperature fluctuation due to the gravity wave. The other minimum of the Richardson number is shown at 77.5 km, but this does not seem to be reliable because it occurs near the edge of the region of the model calculation. When there is no gravity wave, the Richardson number due only to the background linear trend is 5 or 6. As is shown in Figure 12, the altitude of the minimum Richardson number is robust and varies less than 200 m as the amplitude or the wavelength of the gravity wave changes up to ±10%. The altitude of the minimum Richardson number is even less sensitive to changes in other parameters. The minimum Richardson number changes sign as the amplitude and the wavelength are varied.

TABLE 2. Parameters for the Richardson Number Calculations

Parameter	Value
Observation period	February 8, 1985
Inertia gravity waves	
Intrinsic period, h	8.0
Vertical wavelength, km	5.6
Propagation direction	7° east from the north
Amplitude,* m s^{-1}	19.0
Mean background wind	
Northward wind	
Shear, m s^{-1} km^{-1}	3.7
Velocity at 70 km, m s^{-1}	−14
Eastward wind	
Shear, m s^{-1} km^{-1}	4.4
Velocity at 70 km, m s^{-1}	13

*Maximum wind velocity along the long axis of the ellipse.

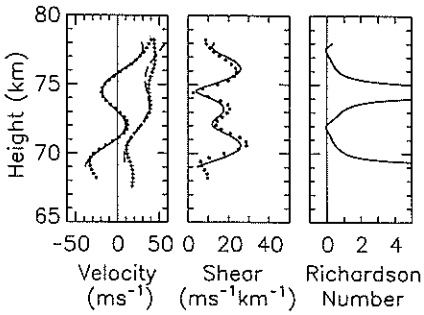

Fig. 11. Vertical profiles of wind fields (left panel), wind shear (center panel), and the Richardson number (right panel). All lines correspond to the calculated profiles obtained by using the simplified wind model shown in Table 2. In the left panel, solid and dashed lines correspond to the northward and eastward components of the wind model, and closed circles and crosses correspond to the northward and eastward wind velocities observed during 1230–1330 LT on February 8, 1985, respectively. Closed circles in the center panel correspond to the intensity of vector wind shear of the observed wind velocity.

As is mentioned above, the wind profile is well described by the single monochromatic inertia gravity wave, the amplitude of which does not increase with altitude. Also, the minimum Richardson number is smaller than the critical value for the onset of shear and convective instabilities. This suggests that the inertia gravity wave is saturated and dissipating its energy. The minimum value of the Richardson number at 72 km coincides with an enhancement of the echo power in Figure 9. On the basis of the wavelike structure and small-scale patches in the turbulent layer, the inertia gravity wave seems to induce instabilities that are not observed in the wind velocities and to produce turbulence.

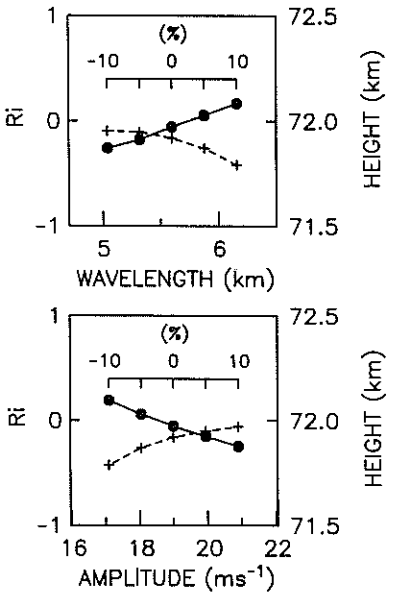

Fig. 12. Variation of the minimum Richardson number (solid line) and its altitude (dashed line) versus parameters of the gravity wave model shown in Table 2. Top and bottom panels correspond to the variations obtained by changing the wavelength and the amplitude of the model up to ±10%, respectively; other parameters are not changed in each case. The symbols at the center of the horizontal range correspond to the minimum Richardson number shown in Figure 11.

The phase reversals of the radial velocity fluctuations, on the other hand, occur at slightly higher altitudes than the altitude of the minimum Richardson number. At the altitude of the phase reversal the calculated Richardson number is slightly larger than $\frac{1}{4}$ but less than 1, and the wind shear is larger than that at the altitude of the minimum Richardson number. It seems possible that the Richardson number at the phase reversal becomes instantaneously less than the critical value of shear or convective instabilities due to the superposition of the smaller-scale perturbation. The rms speed shown in Figure 6 actually shows that the fluctuations occur intermittently. The fluctuation was very similar to that of the Kelvin-Helmholtz instabilities in the troposphere. However, we cannot identify the nature of the fluctuations, because the wind field induced by the inertia gravity wave does not produce a parallel stratified shear flow and instabilities in rotational shear flow have not been studied theoretically. The radial wind fluctuations seem to be due to shear or convective instabilities, with the largest vertical scale among those observed as the echo power enhancement. Although another possibility is that the fluctuation is induced by the parametric instability, it seems to be beyond the scope of these observations to determine the mechanism of the fluctuation.

CONCLUDING REMARKS

MU radar observations of the mesosphere with high time and range resolution have revealed the following points on the behavior of inertia gravity waves and their relationship to the radial wind fluctuations and echo power.

1. An inertia gravity wave has been detected in the wind profile, the intrinsic period and the propagating direction of which are determined by using the linear polarization equations of gravity waves. The amplitude of the inertia gravity wave is comparable to the mean wind velocity. This shows that the stability of the atmosphere should be calculated by taking into account the fluctuation of the potential temperature due to gravity waves.

2. We have found that the inertia gravity wave is saturated and generates turbulence through instabilities, because the minimum Richardson number due to the gravity wave was slightly negative, and the turbulence echo power showed a peak at the altitude of the minimum.

3. In the radial wind velocities we have found fluctuations with a period of 9 min which show a rapid phase reversal near the minimum Richardson number. Although the fluctuations were very similar to the Kelvin-Helmholtz instabilities observed in the troposphere, it is possible that they were induced by the convective or parametric instability.

In this paper we have been able to show clear evidence that gravity waves are saturated and induce instabilities in the mesosphere. As is shown by *Yamamoto et al.* [1987], we frequently find scattering layers which are associated with the inertia gravity waves. This kind of wave may possibly be one of the energy sources in the mesosphere. In order to reveal the acceleration of the mean wind and the energy sources in the mesosphere it will be necessary to investigate the momentum flux and the statistical characteristics of gravity waves.

Acknowledgments. The authors thank T. E. VanZandt, D. C. Fritts, and J. Klostermeyer for helpful discussions and suggestions. The authors are also grateful to B. H. Briggs and to W. L. Oliver, Jr., for his careful reading of the manuscript. The MU radar belongs to and is operated by the Radio Atmospheric Science Center, Kyoto University. Some of computations in the present work have been done at the Data Processing Center of Kyoto University.

REFERENCES

Drazin, P. G., The stability of a shear layer in an unbounded heterogeneous inviscid fluid, *J. Fluid Mech., 4*, 214–224, 1958.

Fritts, D. C., and P. K. Rastogi, Convective and dynamical instabilities due to gravity wave motions in the lower and middle atmosphere: Theory and observations, *Radio Sci., 20*, 1247–1277, 1985.

Fukao, S., T. Sato, S. Kato, R. M. Harper, R. F. Woodman, and W. E. Gordon, Mesospheric winds and waves over Jicamarca on May 23–24, 1974, *J. Geophys. Res., 84*, 4379–4386, 1979.

Fukao, S., T. Sato, T. Tsuda, S. Kato, K. Wakasugi, and T. Makihira, The MU radar with an active phased array system, 1, Antenna and power amplifiers, *Radio Sci., 20*, 1155–1168, 1985*a*.

Fukao, S., T. Tsuda, T. Sato, S. Kato, K. Wakasugi, and T. Makihira, The MU radar with an active phased array system, 2, In-house equipment, *Radio Sci., 20*, 1169–1176, 1985*b*.

Gossard, E. E., and W. H. Hooke, *Waves in the Atmosphere*, pp. 111–121, Elsevier, New York, 1975.

Hodges, R. R., Jr., Generation of turbulence in the upper atmosphere by internal gravity waves, *J. Geophys. Res., 72*, 3455–3458, 1967.

Kato, S., *Dynamics of the Upper Atmosphere*, pp. 93–95, D. Reidel, Hingham, Mass., 1980.

Kato, S., T. Ogawa, T. Tsuda, T. Sato, I. Kimura, and S. Fukao, The middle and upper atmosphere radar: First results using a partial system, *Radio Sci., 19*, 1475–1484, 1984.

Klostermeyer, J., and R. Rüster, Radar observation and model computation of a jet stream–generated Kelvin-Helmholtz instability, *J. Geophys. Res., 85*, 2841–2846, 1980.

Klostermeyer, J., and R. Rüster, Further study of a jet stream–generated Kelvin-Helmholtz instability, *J. Geophys. Res., 86*, 6631–6637, 1981.

Klostermeyer, J., and R. Rüster, VHF radar observation of wave instability and turbulence in the mesosphere, *Adv. Space Res., 4*, 79–82, 1984.

Lindzen, R. S., Turbulence and stress owing to gravity wave and tidal breakdown, *J. Geophys. Res., 86*, 9707–9714, 1981.

Manson, A. H., C. E. Meek, and R. J. Stening, The role of atmospheric waves (1.5 h–10 days) in the dynamics of the mesosphere and lower thermosphere at Saskatoon (52°N, 107°W) during four seasons of 1976, *J. Atmos. Terr. Phys., 41*, 325–335, 1979.

Rastogi, P. K., and S. A. Bowhill, Gravity waves in the equatorial mesosphere, *J. Atmos. Terr. Phys., 38*, 51–60, 1976.

Tsuda, T., K. Hirose, S. Kato, and M. P. Sulzer, Some findings on correlation between the stratospheric echo power and the wind shear observed by the Arecibo UHF radar, *Radio Sci., 20*, 1503–1508, 1985.

VanZandt, T. E., J. L. Green, W. L. Clark, and J. R. Grant, Buoyancy waves in the troposphere: Doppler radar observations and a theoretical model, *Geophys. Res. Lett., 6*, 429–432, 1979.

Vincent, R. A., Gravity-wave motions in the mesosphere, *J. Atmos. Terr. Phys., 46*, 119–128, 1984.

Vincent, R. A., and T. J. Stubbs, A study of motions in the winter mesosphere using the partial reflection drift technique, *Planet. Space Sci., 25*, 441–455, 1977.

Yamamoto, M., T. Tsuda, S. Kato, T. Sato, and S. Fukao, Interpretation of the structure of mesospheric turbulence layers in terms of inertia gravity waves, *Phys. Scr.*, in press, 1987.

S. Fukao, S. Kato, T. Sato, T. Tsuda, and M. Yamamoto, Radio Atmospheric Science Center, Kyoto University, Uji, Kyoto 611, Japan.

(Received February 12, 1987;
revised April 14, 1987;
accepted June 30, 1987.)